INTERPLAY BETWEEN STRUCTURAL AND ELECTRONIC PROPERTIES OF CARBON NANOTUBES

DAVID TOMÁNEK
Department of Physics and Astronomy and
Center for Fundamental Materials Research,
Michigan State University, East Lansing, Michigan 48824-1116, USA
E-mail: tomanek@msu.edu

A combination of *ab initio* Density Functional and parametrized Linear Combination of Atomic Orbitals calculations is used to describe the interplay between structural and electronic properties of single-wall, multi-wall, and bundled carbon nanotubes. The electronic structure of cylindrical single-and multi-wall tubes with an extremely inhomogeneous charge density is determined self-consistently using a new technique that discretizes the eigenvalue problem on a grid and yields simultaneously all occupied and unoccupied states. Comparison with parametrized calculations, which consider explicitly the atomic positions, proves that the essential features of the electronic structure in these systems can be obtained if the ionic background is approximated by infinitely thin structureless cylindrical walls. Consideration of the atomic positions is essential when describing the low-frequency twisting motion of individual tubes within a "rope" or a multi-wall nanotubes. It is shown that the weak, partly anisotropic inter-wall interaction may cause significant changes in the density of states near the Fermi level in these systems.

1 Introduction

Carbon nanotubes, consisting of graphite layers wrapped into seamless cylinders, have been produced in the carbon arc and by laser vaporizing graphite [1,2,3,4,5,6]. Both single-wall and multi-wall systems have been observed that are up to a fraction of a millimeter long, yet only nanometers in diameter. The outer tube diameter varies typically between $2-20$ nm, while the inner diameter is typically of the order of $1-3$ nm. The interlayer distance of $\approx$0.34 nm is close to that of graphite. Absence of defects and chemical inertness suggests that these molecular conductors should be ideal candidates for use as nano-wires.

The first problem, addressed in this study, is related to the electronic structure of nanotubes. The previous success of the jellium model describing the electronic structure and abundance of nanometer-sized alkali clusters suggests that atomic positions may not play a significant role when describing the electronic structure of carbon nanotubes and related one-dimensional systems.

On the other hand, theoretical studies have shown that the diameter and chirality do have a profound effect on the electronic structure of isolated single-wall nanotubes [7,8]. Parametrized calculations addressing only the $pp\pi$ inter-

atomic interactions, which dominate the electronic structure near the Fermi level, indicated that the achiral "armchair" (n, n) nanotubes [9] should be metallic, whereas all (n, m) tubes, with $n - m$ a nonzero multiple of three, should be small gap semiconductors or semimetals [7]. Nanotubes not fitting in either category should be semiconducting, with a band gap roughly proportional to the reciprocal tube radius [10]. These findings have been confirmed in tubes with a large diameter, where the sp^3 bonding contribution is negligible [11].

As the first topic, this study addresses the adequacy of either approach in complex systems consisting of several nanotubes. It focuses on multi-wall and bundled nanotubes, and discusses how the electronic structure of these systems evolves from that of single-wall nanotubes. A self-consistent calculation of the charge distribution in such layered systems turns out to be very difficult, since the determination of eigenstates tends to be either numerically unstable, or fails to reproduce the inter-layer states correctly. Here we review a recently published approach [12] which addresses these problems in systems with cylindrical symmetry. This approach, which is outlined in the following Section, is based on a numerical method introduced by Salomonson and Öster [13], that had been originally developed to treat correlation effects in many-body calculations of atoms.

A second problem, addressed in this study, concerns the interplay between structural and electronic properties of systems consisting of many nanotubes. The spherical counterparts of nanotubes, fullerenes such as C_{60}, have been observed to spin within the C_{60} solid, whereas spinning or twisting of individual tubes within a bundle or a multi-wall tube has not been discussed so far. Our particular interest in tube rotations results from the fact that both the spinning/twisting motion and the electronic structure of these systems depends strongly on the anisotropy of the inter-tube interaction. We suggest the onset of "orientational melting" at T^* as one possible explanation of the unusual temperature dependence of resistivity in nanotube bundles, which show a transition from non-metallic to metallic behavior as the sign of $d\rho/dT$ changes at $T^* \approx 50 - 100$ K.

2 Theory

In the following we discuss two possible approaches to determine the electronic structure of nanotubes and related systems with near-cylindrical symmetry.

First, we review a recently published [12], numerically stable formalism to study the electronic structure of single-wall, multi-wall, and filled carbon nanotubes as well as nanowires. This general, self-consistent approach, based on the *ab initio* density functional formalism, yields the complete spectrum of oc-

cupied and unoccupied eigenstates in systems with cylindrical symmetry. We apply this technique to the above-mentioned systems with extreme spatial variations of the charge density, treating the ionic background in an approximative way.

In the second part, we will review the parametrized Linear Combination of Atomic Orbitals technique that will allow us to assess the effect of the exact ionic positions on the electronic structure of a nanotube systems.

2.1 Density functional calculation of the complete set of electronic eigenstates of nanotubes

The numerical procedure to calculate self-consistently the electronic structure of nanotubes follows closely that described in Ref. [12] and is based on the density functional theory (DFT) [14,15]. All expressions, unless their dimension is specified, will be given in Hartree atomic units.

In the electronic ground state, the total energy E is a well-defined functional of the total charge density $\rho(\mathbf{r})$. $E[\rho(\mathbf{r})]$ can then be obtained in a variational manner, with the constraint that the total number of electrons be conserved, by solving self-consistently the set of Kohn-Sham equations [15]

$$\left[-\frac{1}{2}\nabla^2 + V_{eff}(\mathbf{r})\right]\psi_i(\mathbf{r}) = \varepsilon_i\,\psi_i(\mathbf{r})$$
$$\rho(\mathbf{r}) = \sum_{\mathbf{i}}^{\mathbf{occ}} |\psi_{\mathbf{i}}(\mathbf{r})|^{\mathbf{2}}\,. \tag{1}$$

The effective potential V_{eff} in the local density functional (LDA) formalism is given by

$$V_{eff}(\mathbf{r}) = V_{ion}(\mathbf{r}) + V_H\left(\rho(\mathbf{r})\right) + V_{xc}\left(\rho(\mathbf{r})\right)\,, \tag{2}$$

where V_{ion} is the ionic background potential, V_H is the Hartree potential, and V_{xc} is a local potential describing the effect of exchange and correlation. In the present work, we use the Gunnarsson-Lundqvist parameterization [16] of V_{xc}.

The most satisfying approach to determining the electronic states of multiwall nanotubes would be to consider their atomic structure. This could be achieved in a self-consistent manner using LDA with a Linear Combination of Atomic Orbitals (LCAO) basis. However, the large number of carbon atoms per unit cell needed to describe a long, possibly chiral nanotube makes a simplified approach more attractive. In the following, we focus on the electronic structure arising from the interacting $2s$ and $2p$ valence electrons of carbon, and replace the point charges of the individual C^{4+} ions in the graphitic walls by two-dimensional charged "sheets" ("2D jellium background") of cylindrical

symmetry, with uniform surface-charge density σ. For a graphitic honeycomb lattice with a C–C bond length of 2.68 a.u. we obtain $\sigma = +0.428$ e/a.u.^{2}.

Eigenvalue problem in systems with cylindrical symmetry The potential due to the ionic background charge of an infinitely long single-wall nanotube of radius R is given by Gauss's law [17] as

$$V_{ion}(r) = \begin{cases} -2\lambda \log(R) + c \text{ for} & r \leq R \\ -2\lambda \log(r) + c \text{ for} & r > R \,, \end{cases} \tag{3}$$

where $\lambda = 2\pi R\sigma$ is the number of electrons per unit length of the nanotube and c is an arbitrary constant. In multi-wall nanotubes the total ionic background potential is a superposition of potentials obtained using Eq. (3) for the individual nanotubes of radius R. Gauss' law gives also a very similar expression for the ionic background potential of an infinitely long, structureless solid wire of radius R,

$$V_{ion}(r) = \begin{cases} -\lambda((r/R)^2 - 1) - 2\lambda \log(R) + c \text{ for} & r \leq R \\ -2\lambda \log(r) + c \text{ for} & r > R \,. \end{cases} \tag{4}$$

Here, λ is the number of electrons per unit length of the wire and c is an arbitrary constant. The eigenfunctions of the Kohn-Sham operator for a nanotube or nanowire of length L (with $L >> R$), aligned with the z axis, can be factorized into a radial, an azimuthal, and an axial part as

$$\psi_{nmk}(r, \varphi, z) = \frac{1}{\sqrt{\pi L}} R_{nm}(r) e^{im\varphi} \sin\left(\frac{k\pi}{L} z\right) \,. \tag{5}$$

Here, $n = 1, 2, 3, \ldots$ denotes the radial quantum number, $m = 0, \pm 1, \pm 2, \ldots$ the azimuthal quantum number, and $k = 1, 2, 3, \ldots$ the axial quantum number. The physical significance of $(n-1)$ is the number of radial nodes of ψ_{nmk}. In the corresponding fashion, $|m|$ and $(k-1)$ give the number of azimuthal and longitudinal nodes of ψ_{nmk}, respectively.

We now construct a cylindrical box of large but finite length L, and align the axes of the nanotube and the cylinder. The discretization of the spectrum due to the finite length L is minimized for sufficiently large values of L. The most challenging problem is the determination of the radial wavefunction $R_{nm}(r)$, which we solve by first substituting $R_{nm}(r) = u_{nm}(r)/\sqrt{r}$. The Kohn-Sham Eq. (1) leads to a new equation for $u_{nm}(r)$

$$\left[-\frac{1}{2}\left\{\frac{\partial^2}{\partial r^2} + \frac{1}{4r^2}\right\} + \frac{m^2}{2r^2} + \frac{k^2\pi^2}{2L^2} + V_{eff}(r)\right] u_{nm}(r) = \varepsilon_{nmk}\, u_{nm}(r) \,. \tag{6}$$

Numerically stable technique to solve the eigenvalue problem A numerical solution of the differential equation (6) for the radial function $u_{nm}(r)$ using a standard point-and-shoot method [18] generally fails if several classically allowed regions are separated by forbidden regions, which is the case in multi-wall nanotubes. To solve this differential equation, we adopt a technique introduced by Salomonson and Öster [13], that has been originally developed for atoms, to systems with cylindrical symmetry. The objective is to determine the eigenfunction $u_{nm}(r)$ on a linear grid of N points $r_1, \ldots, r_N$, separated by a constant distance h, inside the cylindrical box. To evaluate the kinetic term in the radial Eq. (6), we use the symmetric five-point formula for the second-order derivative of a function $u_{nm}(r)$

$$\frac{\partial^2 u(r)}{\partial r^2} = \frac{1}{12h^2}[-u(r-2h)+16u(r-h)-30u(r)+16u(r+h)-u(r+2h)]+O(h^4) \; . \tag{7}$$

Substituting the expression (7) in Eq. (6) leads to a set of N coupled linear equations for $u_{nm}(r_i)$ that can be formulated as an eigenvalue problem

$$(A + D)\, \mathbf{u_{nm}} = \varepsilon\, \mathbf{u_{nm}} \; . \tag{8}$$

Determining the eigenvector $\mathbf{u} = (u_{nm}(r_1), u_{nm}(r_2), \ldots, u_{nm}(r_N))$ in Eq. (8) is equivalent to solving Eq. (6) on the radial grid. The matrix describing the operator A is diagonal, with its elements given by

$$A_{ii} = \frac{m^2}{2r_i^2} + \frac{k^2\pi^2}{2L^2} + V_{ion}(r_i) + V_H(r_i) + V_{xc}(r_i) \quad , \tag{9}$$

where $i = 1, 2, \ldots, N$. D is the symmetric band matrix obtained from Eq. (7), given by

$$D = -\frac{1}{24h^2} \begin{pmatrix} -30 + \frac{1}{4r_1^2} & 16 & -1 & 0 & 0 & \cdots & 0 \\ 16 & -30 + \frac{1}{4r_2^2} & 16 & -1 & 0 & \cdots & 0 \\ -1 & 16 & -30 + \frac{1}{4r_3^2} & 16 & -1 & \cdots & -1 \\ \vdots & \vdots & \vdots & \vdots & \vdots & \ddots & 16 \\ 0 & 0 & 0 & 0 & -1 & 16 & -30 + \frac{1}{4r_N^2} \end{pmatrix} . \tag{10}$$

We require $A + D$ to be symmetric in order to obtain a real eigenvalue ε in Eq. (8) and a radial eigenfunction $u_{nm}(r)$ that is real and doubly differentiable everywhere inside the cylinder. The above form of D implies that the

wavefunctions vanish outside the grid, i.e. all electrons are contained in the cylindrical box. The asymptotic behavior of $u_{nm}(r)$ in the region close to the z-axis, $u_{nm}(r) \propto r^{|m|+1/2}$, has to be enforced, while still keeping the matrix D symmetric [13]. To achieve this, we focus on the matrix elements D_{11}, D_{12}, D_{21} and D_{22}. The $A + D$ matrix can be symmetrized by extending the radial axis to the left of the first grid point, and using the ansatz

$$\begin{aligned} u_{nm}(r_0) &= \alpha \left[\frac{u_{nm}(r_0)}{u_{nm}(r_1)}\right] u_{nm}(r_1) + (1-\alpha) \left[\frac{u_{nm}(r_0)}{u_{nm}(r_2)}\right] u_{nm}(r_2) \\ u_{nm}(r_{-1}) &= \left[\frac{u_{nm}(r_{-1})}{u_{nm}(r_1)}\right] u_{nm}(r_1) \end{aligned} \tag{11}$$

for the function values at the new grid points r_{-1} and r_0 preceding the first grid point r_1. The function value ratios occurring in Eq. (11) are determined using the appropriate asymptotic behavior of $u_{nm}(r)$. The free parameter α is then chosen in such a way that $D_{12} = D_{21}$.

The last difficulty in the solution of the eigenvalue Eq. (6) occurs due to the divergence of two terms in the differential operator at $r = 0$. We address this problem in systems with nonzero charge density near the cylinder axis by introducing a very fine grid near $r = 0$ and displacing this grid laterally by a small distance, e.g. $0.1h$. In this case, none of the microgrid points $r_{-1} = 0.1h, r_0 = 1.1h, r_1 = 2.1h, \ldots$, coincides with $r = 0$. Interpolation is then used to determine the radial wave function and all its derivatives even in the region close to the cylinder axis.

We note that the total number of eigenstates is determined by the rank N of the matrices A and D in Eq. (8) (that is related to the radial grid) and not the total number of electrons. Consequently, this approach can be used to determine also the unoccupied states, which are the basis of calculations determining the collective response of these systems, e.g. using the time-dependent LDA (TDLDA) or the LDA-based Random Phase Approximation (LDA-RPA) technique.

2.2 Parametrized Linear Combination of Atomic Orbitals (LCAO) technique

To investigate the effect of discrete atomic positions on the electronic structure of nanotubes, we have made use of the parametrized linear combination of atomic orbitals technique, since the full LDA theory is too demanding on computer resources. It has been shown that mapping LDA results for characteristic structures onto parameters of an LCAO Hamiltonian provides a very useful and efficient way to determine the electronic states of carbon systems

[19]. The nearest-neighbor LCAO Hamiltonian we use reads

$$H_{LCAO} = \sum_i \sum_\beta \epsilon^0_{i\beta} a^\dagger_{i\beta} a_{i\beta} + \sum_{i<j} \sum_{\beta,\beta'} t_{i\beta,j\beta'} (a^\dagger_{i\beta} a_{j\beta'} + c.c.) \; . \qquad (12)$$

In the present notation, α and β refer to electronic levels of the cluster and isolated atoms, respectively, and Roman indices denote atomic sites. In the LCAO calculations of carbon nanotubes, we use four orbitals of s, p_x, p_y, and p_z character on each atomic site and Slater-Koster parameters [19] for the matrix elements of the Hamiltonian (12).

3 Results

3.1 Electronic Structure of Isolated Nanotubes

In Fig. 1 we present results for the charge distribution and the total potential of a hollow single-wall nanotube, a thin nanowire, a tube filled by a nanowire, and a double-wall nanotube. In these calculations, the C^{4+} ion charges in each nanotube wall have been smeared out into infinitely thin cylindrical walls, representing a "2D jellium background", and only the C2s and C2p valence electrons have been considered as active. Our description of Pb nanowires within the jellium model follows Ref. [20]. We use $r_s = 2.30$ a.u. for the Wigner-Seitz radius and the valence $Z = 4$ for Pb in the ground-state configuration $[Xe]4f^{14}5d^{10}6s^26p^2$. The jellium background charge density of Bi, which has also been found to fill carbon nanotubes, is only ≈25% higher than in Pb. Consequently, we expect qualitatively similar results for nanowires of these two elements.

As mentioned in the Theory Section, the electronic states in systems with cylindrical symmetry are characterized by the quantum numbers n, m and k, where $(n-1)$ corresponds to the number of radial nodes, $|m|$ corresponds to the number of azimuthal nodes, and $(k-1)$ is the number of longitudinal nodes of the wavefunction. In order to better understand the nature of such wavefunctions in cylindrical symmetry, we first turn to analogous spherical systems, such as the C_{60} fullerene, that have been studied extensively from this point of view.

The C_{60} molecule with icosahedral symmetry contains all sixty atoms in equivalent sites on a hollow, spherical graphitic shell. The near-spherical structure of C_{60} suggests to represent the wave functions in a spherical basis [21]. Indeed, results of self-consistent LDA calculations for C_{60} suggest that to a good approximation, occupied eigenstates of C_{60} can be characterized by radial and angular quantum numbers [22]. The description of C_{60} by a spherically symmetric hollow cage turned out to be a very reasonable first approximation

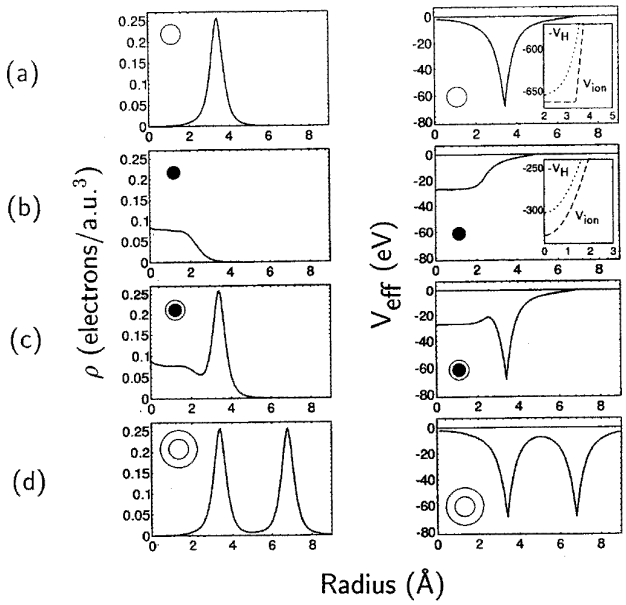

Figure 1: Results for the self-consistent radial charge density $\rho(r)$ and effective total potential $V_{eff}(r)$ of (a) a hollow single-wall carbon nanotube with radius $R = 3.4$ Å, (b) a solid Pb nanowire with $R = 2.4$ Å, (c) the nanowire (b) encapsulated in the nanotube (a), and finally (d) a double-wall nanotube, consisting of the nanotube (a) enclosed inside a nanotube with the radius $R = 6.8$ Å. Symbols are introduced to distinguish the different systems in the subfigures. From Ref. [12]. ©American Physical Society 1997.

that could be further improved systematically by considering correction terms addressing the icosahedral point-group symmetry breaking [23,24]. Since atomic positions are ignored in the spherical hollow cage description of C_{60}, there is no direct way to distinguish the electronic states associated with individual interatomic σ and π bonds. The distinction between the σ and π *states* is rather based on the fact that the graphitic layer is a nodal layer for the nonbonding $pp\pi$ molecular orbitals, whereas it is not a nodal layer for the σ orbitals. Correspondingly, σ states can be associated with wavefunctions that have no radial nodes, whereas π states have a single node in the radial wave function. The angular arrangement of the wavefunction nodes is given by the spherical harmonics and the angular quantum number $l = 0, 1, 2, \ldots$. An analysis of the occupied levels of the C_{60} molecule shows that the levels close to the highest occupied molecular orbital (HOMO) are of π type, whereas the more deeply

bound states are of σ type [25].

Since the interatomic bonding in the nanotubes and the C_{60} fullerene are very similar, we expect that a description of the C^{4+} ions by a homogeneously charged, infinitely thin layer will provide a valid description also for the nanotube. As in the C_{60} molecule, we will distinguish σ states with no radial node from π states with one radial node in the graphene wall. This is illustrated in Fig. 2, which displays the total and partial electronic densities of states (DOS) for the isolated nanotube and the nanowire discussed above and in Fig. 1.

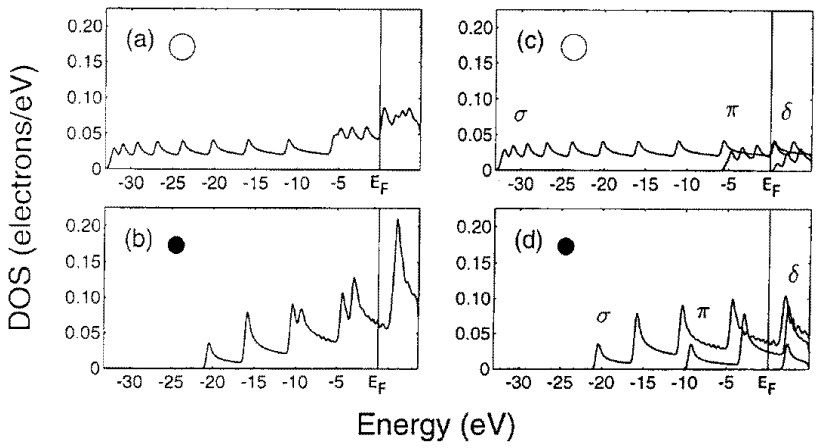

Figure 2: Total electronic density of states (DOS) of (a) a hollow single-wall nanotube with the radius $R = 3.4$ Å, and (b) a solid Pb nanowire with $R = 2.4$ Å, with E_F at energy zero. (c) The partial DOS with respect to the radial quantum number n of the nanotube (a) shows the $n = 1$ (σ), $n = 2$ (π), and $n = 3$ (δ) bands extending above -33 eV, -5 eV, and E_F, respectively. (d) The corresponding partial DOS of the nanowire (b) shows the σ, π, and the δ bands extending above -21 eV, -10 eV, and $+2$ eV, respectively. Symbols are introduced to distinguish the different systems in the subfigures. From Ref. [12].

The comparison between the total DOS for the isolated nanotube in Fig. 2(a) and its decomposition into partial DOS according to the radial wave number n in Fig. 2(c) shows an energy level spectrum starting 33 eV below the Fermi level with states containing no radial nodes, establishing that bonding originates from the σ states. The π states are much higher in energy and close to the Fermi level, establishing their essentially nonbonding character. None of the $n = 3$ (δ) band states is occupied in the ground state, but such states are important when studying electronic excitations. Similarly, our results for the total and partial DOS of the Pb nanowire, shown in Figs. 2(b) and (d), suggest

that only $n = 1$ (σ) and $n = 2$ (π) states are occupied in this system.

Both the nanotube and the nanowire show substructure in the DOS of each $n-$decomposed subband, that is associated with the azimuthal quantum number m and the longitudinal momentum k. The peaks in the partial densities of states are van Hove singularities that occur in one-dimensional systems [20]. Each of these singularities is associated with a particular azimuthal quantum number $|m|$; singularities occurring at higher energies are associated with larger values of $|m|$. We will refer back to Fig. 2 in the following, when discussing the DOS of more complex systems, such as multi-wall and filled nanotubes.

The van Hove singularities, which are typical of one-dimensional systems and dominate the density of states of the "2D jellium background" nanotube in Fig. 2(a), as well as the azimuthal subbands in Fig. 2(c), are also present when the discrete atomic positions are considered in the electronic structure calculation. This means that the parametrized LCAO technique reflects correctly the one-dimensional axial as well as the radial and azimuthal states. We conclude that both techniques yield electronic spectra that can be characterized by the radial, azimuthal, and axial quantum numbers n, m and k, with consistent level ordering.

3.2 Effect of Inter-Tube Interactions on the Electronic Structure

In the following, we focus the on the effect of inter-wall coupling on the electronic structure of multi-wall and bundled single-wall nanotubes. These small effects are addressed using a combination of *ab initio* and parametrized techniques. To obtain the total energy of nanotubes in perfect lattices or of fragments near the tube end, we use the Density Functional Formalism with a plane wave basis for the solid [26] and a numerical basis for the fragments [27]. Band structure details are studied using a parametrized Linear Combination of Atomic Orbitals (LCAO) formalism, with parameters described in Ref. [28]. The inter-tube interaction is described in analogy to the inter-ball interaction in the doped C_{60} solid [29]. Up to $102,400$ k-points in the irreducible Brillouin zone are used to determine the electronic structure of ordered nanotube lattices, the "ropes" [26].

Single-Wall Nanotube "Ropes" The interaction between adjacent nanotubes in a bundle or "rope" is, same as in the C_{60} solid, not completely isotropic about the tube axis. Individual (10,10) tubes are expected to librate about their axis with a relatively low frequency of $50 - 60$ cm^{-1}, close to the observed (but not identified) 41 cm^{-1} infrared-active mode[30]. Even though the activation barrier for free rotation is only $\lesssim$4 meV *per atom*, individual tubes

are not expected to rotate rigidly due to their high total mass. Since the rigidity of nanotubes is limited, finite segments are more likely to twist about the tube axis. The twisting motion is likely to be accompanied by displacement of orientational dislocations that have been frozen in during the assembly of the "ropes".

Inter-tube interactions in the ropes have been shown to modify the electronic structure of individual tubes by opening a pseudo-gap near the Fermi level [26,31,32]. With the onset of orientational melting, one would expect the pseudo-gap to smear out, thus significantly increasing the conductivity of the system.

Inter-tube coupling leads to an increase in the density of states by ≈7% outside the pseudo-gap. An even larger increase in the density of states, namely by a factor of ≈12 with respect to the pristine system, is predicted for the potassium doped system with the composition KC_8, in agreement with the observed conductivity increase by a factor of 10∼20 [33].

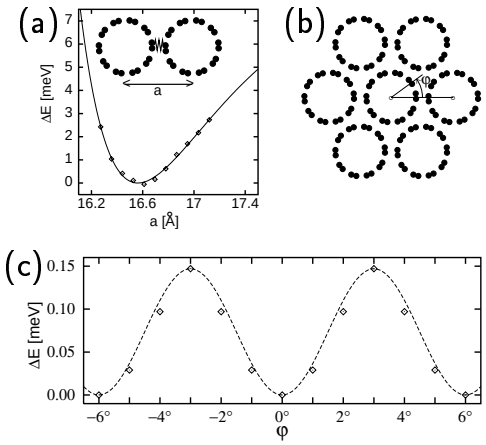

Figure 3: (a) Density functional results for the relative total energy ΔE of a "rope" of (10,10) carbon nanotubes as a function of the inter-tube spacing a. raphite as a function of the bond length d_{CC}. (b) Schematic end-on view of the equilibrium "rope" structure, depicting the tube orientation angle φ. (c) Dependence of the "rope" energy ΔE on the orientation angle φ of individual nanotubes. All energies are given per atom. From Ref. [26]. ©American Physical Society 1998.

Multi-Wall Nanotubes Inter-wall interaction in a multi-wall nanotube may cause similar changes in the electronic structure near the Fermi level as

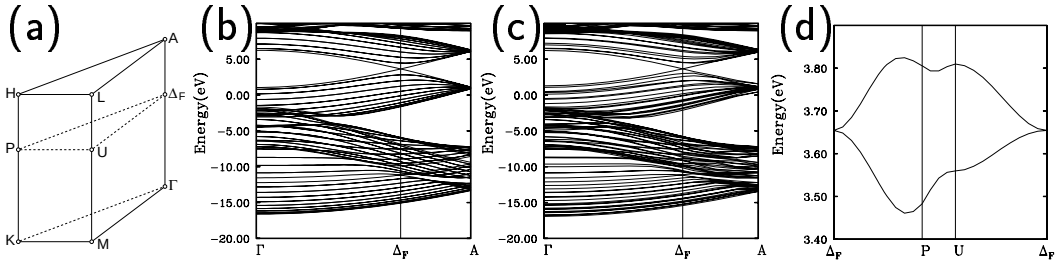

Figure 4: (a) Irreducible part of the hexagonal Brillouin zone of a nanotube crystal, the "rope". Band structure of (b) an individual nanotube and (c) the "rope", along the tube axis. (d) Dispersion of the top valence and bottom conduction bands of the "rope", in a plane perpendicular to the tube axis, containing the point Δ_F depicted in (c). From Ref. [26]. ©American Physical Society 1998.

the inter-tube interaction in "ropes" of nanotubes described above[34,35]. Our calculation for the (5,5)@(10,10) double-wall tube[36] suggests that due to inter-tube coupling, the density of states near E_F increases by $\approx$3%. The value of the rotational barrier *per atom* in this system is somewhat smaller than in nanotube "ropes", in agreement with results for the same system published in Ref. [37]. Off-axis displacements of $\lesssim$0.1 Å in multi-wall tubes cost essentially no energy. For the particular (5,5)@(10,10) double-tube, we expect librational modes to occur at $\omega_{in}\approx$31 cm^{-1} for the inner tube and $\omega_{out}\approx$11 cm^{-1} for the outer tube, depending on which of these tubes is pinned. As in the case of nanotube "ropes", we expect segments of individual tubes to exhibit a twisting motion rather than the entire tubes to rotate rigidly. We also expect an orientational melting transition to occur in multi-wall nanotubes, close to or below the temperature expected in single-wall nanotube "ropes".

4 Summary

We have used the *ab initio* local density functional and parametrized LCAO formalism to study the electronic structure of individual single-, multi-wall, and filled nanotubes, as well as ordered nanotubes lattices.

In most cases, describing nested carbon nanotubes by smearing out the C^{4+} ion charges in the graphene layers into "2D jellium background" cylinders and treating the active C2s and C2p electrons self-consistently proved adequate for the calculation of the electronic structure. In order to handle the extremely inhomogeneous system of multi-wall tubes with $10^3 - 10^4$ electrons, a new formalism has been utilized that discretizes the eigenvalue problem on a grid and yields a *complete* set of occupied and unoccupied states. The self-consistent electronic structure of infinitely long nanotubes, represented by the "2D jellium

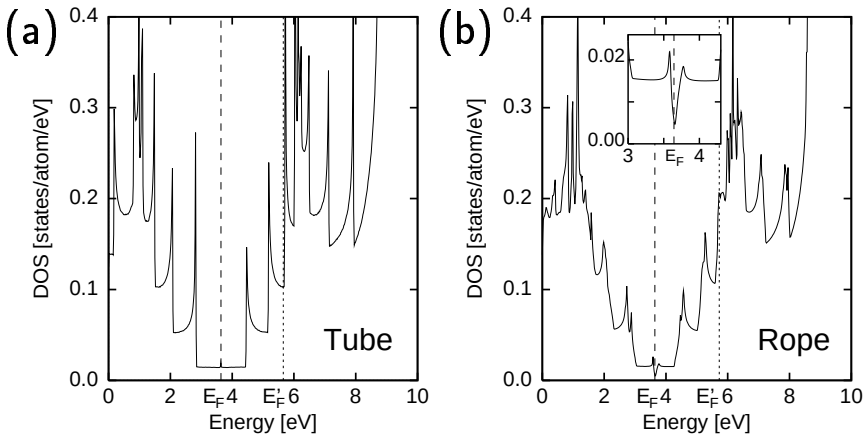

Figure 5: Density of states of (a) an isolated nanotube and (b) a nanotube crystal, the "rope". The structure of the pseudo-gap in the "rope" is displayed in the inset on an expanded energy scale. Dashed and dotted lines indicate the position of the Fermi level E_F for the undoped and E'_F for the KC_8 doped systems, respectively. From Ref. [26]. ©American Physical Society 1998.

background" model, compares favorably with parametrized LCAO calculations that take atomic structure into account. The electronic spectra of single-wall, multi-wall, and filled nanotubes, as well as nanowires, can be characterized by the radial, azimuthal and axial quantum numbers n, m and k. These quantum numbers are reflected in our results based on the self-consistent "2D jellium background" model and the parametrized LCAO technique that considers the atomic structure.

Due to their large inertia, individual nanotubes do not rotate as a whole when they are part of a multi-tube system. Finite tube segments are rather expected to exert a local twisting motion. Orientational dislocations, which were frozen in during the formation of the "ropes", lower the activation barrier for tube rotations and hence the orientational melting temperature of the "ropes". We find that the inter-tube interaction, found in multi-wall nanotubes and ordered "ropes", induces additional band broadening by $\approx$0.2 eV, and opens up a pseudo-gap at E_F in the "ropes" and multi-wall nanotubes.

Acknowledgement

The author gratefully acknowledges financial support by the organizers of the International Workshop on "Collective Excitations in Fermi and Bose Systems" in Serra Negra, Sao Paulo, Brazil, September 14 - 17, 1998. Contributions of Young-Kyun Kwon, Young Hee Lee, Kee Hag Lee, Susumu Saito, Daniel Östling, Arne Rosén, P.G. Reinhard, Sten Salomonson, and Håkan Warston to this work are gratefully acknowledged.

References

1. S. Iijima, Nature **354**, 56 (1991).
2. S. Iijima and T. Ichihashi, Nature **363**, 603 (1993).
3. D.S. Bethune, C.H. Kiang, M.S. de Vries, G. Gorman, R. Savoy, J. Vazquez, R. Beyers, Nature **363**, 605 (1993).
4. R.E. Smalley, Mat. Sci. Eng. **B 19**, 1 (1993).
5. A. Thess, R. Lee, P. Nikolaev, H. Dai, P. Petit, J. Robert, C. Xu, Y. H. Lee, S. G. Kim, D. T. Colbert, G. Scuseria, D. Tománek, J. E. Fisher, and R. E. Smalley, Science **273**, 483 (1996).
6. M.S. Dresselhaus, G. Dresselhaus, and P.C. Eklund, *Science of Fullerenes and Carbon Nanotubes* (Academic Press, San Diego, 1996).
7. R. Saito, M. Fujita, G. Dresselhaus and M.S. Dresselhaus, Appl. Phys. Lett. **60**, 2204 (1992).
8. N. Hamada, S. Sawada and A. Oshiyama, Phys. Rev. Lett. **68**, 1579 (1992).
9. M.S. Dresselhaus, G. Dresselhaus, and P.C. Eklund, *Science of Fullerenes and Carbon Nanotubes* (Academic Press, San Diego, 1996).
10. J.W. Mintmire, D.H. Robertson, B.I. Dunlap, R.C. Mowrey, D.W. Brenner and C.T. White, Mater. Res. Soc. Sym. Proc. **247**, 339 (1992).
11. X. Blase, L.X. Benedict, E.L. Shirley and S.G. Louie, Phys. Rev. Lett. **72**, 1878 (1994).
12. D. Östling, D. Tománek, and A. Rosén, Phys. Rev. B **55**, 13980 (1997).
13. S. Salomonson and P. Öster, Phys. Rev. A **40**, 5559 (1989).
14. P. Hohenberg and W. Kohn, Phys. Rev. B **136**, 864 (1964).
15. W. Kohn and L.J. Sham, Phys. Rev. A **140**, 1133 (1965).
16. O. Gunnarsson, B.I. Lundqvist, Phys. Rev. B **13**, 4274 (1976).
17. J.D. Jackson, *Classical Electrodynamics*, Second Ed., John Wiley and Sons, New York, 1975.
18. S.E. Koonin, *Computational Physics* (The Benjamin/Cummings Publishing, Menlo Park, 1986).
19. David Tománek and Michael A. Schluter, Phys. Rev. Lett. **67**, 2331

(1991).
20. N.W. Ashcroft and N.D. Mermin, *Solid State Physics*, Saunders College Publishing, 1976.
21. M. Braga, S. Larsson, A. Rosén and A. Volosov, Astron. Astrophys. **245**, 232 (1991).
22. J.L. Martins, N. Troullier and J.H. Weaver, Chem. Phys. Lett. **180**, 457 (1991).
23. K. Yabana and G.F. Bertsch, Physica Scripta **48**, 633 (1993).
24. C. Yannouleas and U. Landman, Chem. Phys. Lett. **217**, 175 (1994).
25. E. Westin and A. Rosén, Int. J. Mod. Phys. B **6**, 3893 (1992).
26. Young-Kyun Kwon, Susumu Saito, and David Tománek Phys. Rev. B - Rapid Communications (October 15, 1998); Young-Kyun Kwon, David Tománek, Young Hee Lee, Kee Hag Lee, and Susumu Saito, J. Mater. Res. **13**, 2363 (1998).
27. Young Hee Lee, Seong Gon Kim, and David Tománek, Phys. Rev. Lett. **78**, 2393 (1997).
28. D. Tománek and Michael A. Schlüter, Phys. Rev. Lett. **67**, 2331 (1991).
29. M. Schlüter, M. Lannoo, M. Needels, G.A. Baraff, and D. Tománek, Phys. Rev. Lett. **68**, 526 (1992).
30. W. Holmes, J. Hone, R. Mallozzi, J. Orenstein, P.L. Richards, and A. Zettl (private communication).
31. J.-C. Charlier, X. Gonze, and J.-P. Michenaud, Europhys. Lett. **29**, 43 (1995).
32. P. Delaney, H.J. Choi, J. Ihm, S.G. Louie, and M.L. Cohen, Nature **391**, 466 (1998).
33. R.S. Lee, H.J. Kim, J.E. Fischer, A. Thess, and R.E. Smalley, Nature **388**, 255 (1997).
34. Ph. Lambin, L. Philippe, J.C. Charlier, and J.P. Michenaud, Comp. Mat. Sci. **2**, 350 (1994).
35. Ph. Lambin, J.C. Charlier, and J.P. Michenaud, in *"Electronic Properties of Novel Materials"*, edited by H. Kuzmany, J. Fink, M. Mehring and S. Roth (World Scientific, Singapore, 1994), p. 130.
36. Young-Kyun Kwon and David Tománek (submitted for publication).
37. J.C. Charlier and J.P. Michenaud, Phys. Rev. Lett. **70**, 1858 (1993).